# Numerical and experimental investigation of the thermal behavior and microstructure of wire arc additive manufactured 316L stainless steel straight wall part



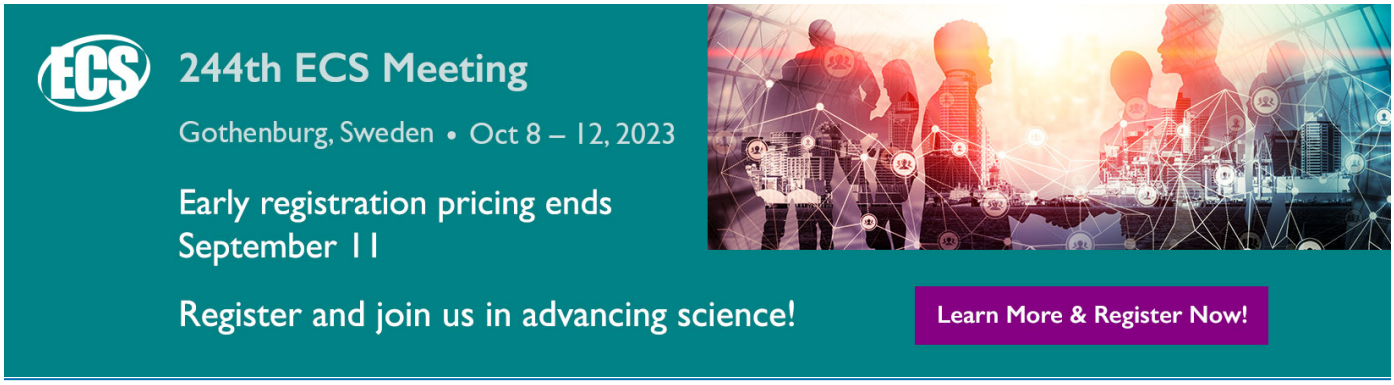

# Numerical and experimental investigation of the thermal behavior and microstructure of wire arc additive manufactured 316L stainless steel straight wall part

**Y Y Di, Z Z Zheng*, S Y Pang and J J Li**
State Key Laboratory of Materials Processing and Die & Mould Technology, Huazhong University of Science and Technology, Wuhan 430074, P.R. China
*Corresponding author, E-mail: zzz@mail.hust.edu.cn

**Abstract.** The heat transfer behavior during wire arc additive manufacturing is closely related to the dimensional accuracy and performance of the formed part. To investigate the thermal behavior of stainless steel 316L straight wall part fabricated by the wire arc additive manufacturing process, a three-dimensional transient finite element model is established based on the double elliptic heat source model. At the same time, the temperature measurement experiment on the characteristic position of the substrate is carried out. The thermal cycle curve obtained by the finite element model is in good agreement with the measured result. By analyzing the simulation results, the finite element model established can effectively reveal the thermal behaviors such as melting, solidification, heat accumulation and remelting during the forming process of the straight wall part. In addition, the solidification parameters obtained by the model are correlated with the microstructure. High G/R induces the production of cellular crystals and columnar dendrites, on the contrary, the formation of equiaxial crystals, which provide guidance for the prediction of the morphology of the microstructure.
**Keywords.** wire arc additive manufacturing; finite element analysis; temperature field; interlayer residence time; microstructure characteristic

## 1. Introduction

Wire arc additive manufacturing (WAAM) can repair or directly fabricate metal parts with the arc as the heat source, which is not limited by the size and structural complexity of the formed metal parts. With high flexibility, high efficiency, and low cost, it has been promising in the forming of large metal parts in the fields of aviation, aerospace, and nuclear power[1, 2]. However, during the deposition process, the previous layers can undergo multiple heating and cooling, and even remelting[3]. The complex thermal cycling process leads to an inhomogeneous structure and performance of the formed parts[4, 5], as well as the generation of defects[6, 7], which may greatly degrade the quality of the parts. Therefore, it is essential to explore the thermal behavior of the deposited layers based on the long-term development of wire arc additive manufacturing technology.

The thermal behavior of the WAAM process is extremely complicated. It is difficult to reveal the real-time temperature evolution characteristics of the deposited parts by temperature measurement experiments with a thermal imager or thermocouple equipment, while the simulation calculation technology can overcome this challenge. In recent years, many researchers have done a lot of work on investigating the thermal behavior of the wire arc additive manufacturing process by using numerical simulation technology. Zhao et al. [8] proposed a 3D transient heat transfer numerical model with temperature-dependent material properties to investigate the effect of deposition orientation on the thermal process during rapid prototyping of single-pass multilayer welds. Ogino et al. [9] evaluated the effect of forming conditions on deposition shape by a combination of experiments and simulations and

demonstrated that the gas metal arc welding (GMAW) melt pool model is a useful tool for predicting and controlling the WAAM process. Xiong et al. [10] investigated the effect of substrate preheating on the thermal behavior of a single pass ten-layer circular component deposited by GMAW by developing a three-dimensional transient heat transfer model. Lei et al. [11] investigated the effect of interlayer residence time on the evolution of the temperature field of an arc additive thin-walled cylindrical component. Zhao et al. [12] used a finite element model to analyze the different stages of the thermal cycle of a shell-shaped component. Hejripour et al. [13] established a three-dimensional numerical heat transfer model to analyze the temperature history and cooling rate of the deposited layers of 2209 duplex stainless steel, and found that a slow cooling rate at high temperatures can significantly promote the formation of austenite in the ferrite matrix. Ou et al. [14] developed three-dimensional heat transfer and fluid flow model to study the effects of arc power, travel speed and wire feed rate on temperature gradient and solidification rate during a single-track H13 tool steel deposition. Huang et al. [15] studied the influence of deposition path on temperature, stress and deformation by establishing a numerical model, and found that the deformation in the same deposition direction was larger than that in the opposite direction, and the distribution of reverse stress was more uniform than that in the same direction. Although a great deal of work has been carried out on the influence of process parameters on the evolution of temperature and stress during the WAAM, further research is needed on the internal relationship between heat transfer behavior, solidification behavior and microstructure in the deposition. In this paper, a three-dimensional transient heat transfer finite element model of the WAAM process is developed using a combination of experimental and computational methods. The temperature distribution, thermal cycle characteristics, solidification parameters and the evolution of microstructure at different interlayer residence times during the deposition are investigated.

## 2. Experiment and materials

The equipment used for the experiments was mainly a CMT 4000 Advanced welder and a KUKA 6-axis robot. The wire material was stainless steel 316L with a diameter of 1.2 mm and the composition is shown in table 1. The straight wall part was deposited on the stainless steel 316LN plate. The length, width, and height of the plate are 200 mm, 150 mm, and 15 mm respectively. The schematic diagram of the WAAM process is shown in figure 1. The straight wall part is deposited on the substrate in a round trip fashion, from the bottom to the top. After each layer was deposited, there was a residence time to help the part transfer excess heat to the environment. The main process parameters are shown in table 2. The straight wall part was obtained by cutting the middle position of the straight arm to obtain the microstructure characteristics of each layer. After being inlaid, ground and polished, the specimen was electrochemically etched in 10% oxalic acid solution and the microstructure was observed using a three-dimensional ultra-depth of field microscope (VHX-1000C).

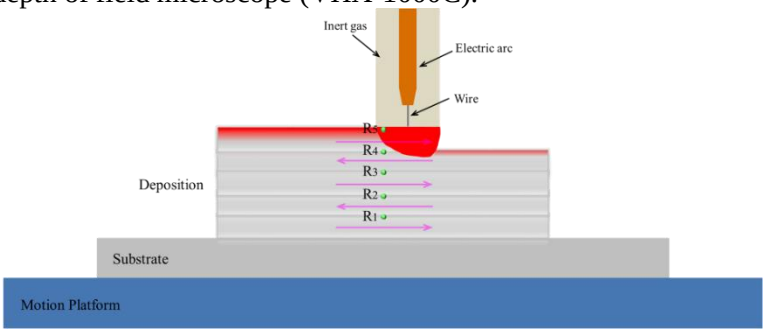


**Figure 1.** Schematic diagrams of the WAAM process.

**Table 1.** Chemical composition of the stainless steel 316L (mass fraction, %).

| C | Si | Mn | P | S | Ni | N | Cr | Mo | Fe |
|---|---|---|---|---|---|---|---|---|---|
| 0.02 | 0.81 | 1.69 | 0.015 | 0.015 | 12.5 | 0.013 | 18.39 | 2.25 | Bal. |

**Table 2.** Experimental parameters of the WAAM process.

| Parameters | Value |
|---|---|
| Voltage (V) | 23.7 |
| Current (A) | 214 |
| Deposition speed (m/min) | 0.6 |
| Wire feed speed (m/min) | 8 |
| Shielding gas | 80%Ar+20%$CO_2$ |
| Gas flow rate (L/min) | 20 |
| Interlayer residence time (s) | 70, 250, 300,200 |

## 3. Numerical simulation

The finite element model was used to explore the thermal behavior in the wire arc additive manufacturing process. The geometric model is established according to the actual size of the straight arm. In the simulation, the time and space movement of the heat source is realized by using life-and-death element technology. In the finite element calculation process, node heat transfer. To improve the accuracy of calculation, relatively small grids were divided in and near the deposition layer.

The Goldack double ellipsoid heat source model [16] is adopted to express the energy generated by the arc as a moving body heat source, where the heat flow density function of the front part of the double ellipsoidal heat source is:

$$q_f(x,y,z)=\frac{6\sqrt{3}f_fQ}{a_fbc\pi\sqrt{\pi}}exp\left(-\frac{3x^2}{a_f^2}-\frac{3y^2}{b^2}-\frac{3z^2}{h^2}\right) \tag{1}$$

The heat flux function of the latter half of the double ellipsoid heat source is:

$$q_r(x,y,z)=\frac{6\sqrt{3}f_rQ}{a_rbc\pi\sqrt{\pi}}exp\left(-\frac{3x^2}{a_r^2}-\frac{3y^2}{b^2}-\frac{3z^2}{h^2}\right) \tag{2}$$

where, $Q$ is the effective heat input, $a_f$ is the length of the semi-axis of the front ellipsoid, $a_r$ is the length of the semi-axis of the rear ellipsoid, $b$ is the width of the heat source, $h$ is the depth of the heat source, $f_f$ is the energy distribution coefficient of the heat input in front of the heat source, $f_r$ is the energy distribution coefficient of the heat input in rear of the heat source.

The analysis of the temperature field in the WAAM process is a typical nonlinear transient heat conduction problem, so the three-dimensional transient heat transfer equation is established:

$$\rho C\frac{\partial T}{\partial t}=\frac{\partial}{\partial x}\left(\lambda\frac{\partial T}{\partial x}\right)+\frac{\partial}{\partial y}\left(\lambda\frac{\partial T}{\partial y}\right)+\frac{\partial}{\partial z}\left(\lambda\frac{\partial T}{\partial z}\right)+Q \tag{3}$$

where, $\rho$ is the mass density, $C$ is the heat capacity, $T$ is the temperature, $\lambda$ is the thermal conductivity.

## 4. Results and discussion

### *4.1. Model validation*

To ensure the reliability of the temperature field results obtained from numerical calculations, the finite element model needs to be validated first. The temperature change profile of the substrate in the wire arc additive manufacturing process is relatively easy to be measured by thermocouples, and the temperature profile obtained from the measurement is verified with the simulation results. The thermal

cycle curves at position A on the substrate obtained from thermocouple measurement and simulation calculation are shown in figure 2. It can be seen that the measured and simulated curves of the temperature change at position A on the plate are in good agreement, and the average error of the temperature is less than 15%, indicating that the established finite element model is effective and can support the study of heat transfer behaviors such as temperature distribution, thermal cycling and solidification characteristics of the formed parts in the WAAM process.

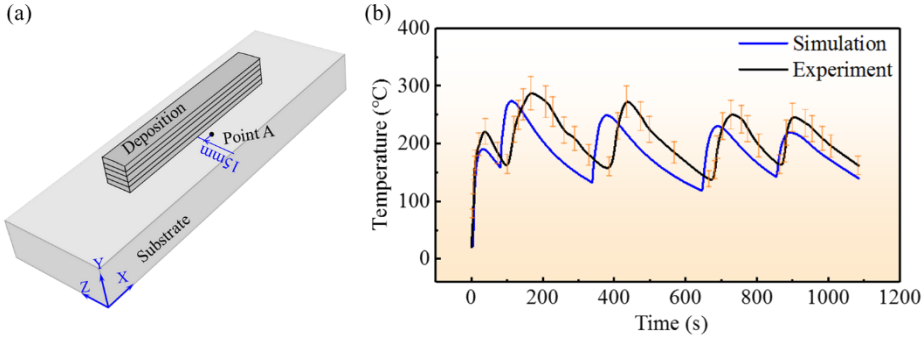


**Figure 2.** Experimental and simulated temperature results:(a) the position of point A; (b) the temperature curve at point A.

*4.2. Heat transfer behavior*

Figure 3 shows the temperature distribution as the heat source passes through the middle of each layer in the WAAM process. It is evident from figure 3 that in the simulation of the additive manufacturing process, the heat source passing through the position cell activation is or has completed the melting and solidification of the metal, and the position not deposited has no cell activation indicating that no metal has been melted and solidified, realizing the forming process of melting and solidification of the metal in the wire arc additive manufacturing technology. The solid white line indicates the liquid level boundary in the melt pool at temperatures above 1450°C. During the deposition process, the temperature field evolves in a consistent pattern for each layer. For each deposited layer, the highest temperature is located near the middle of the top of the melt pool, where heat transfer occurs from the heat source to the surrounding area, with the temperature decreasing as the distance from the substrate decreases. In addition, as the number of deposited layers increases, the degree of heat transfer is higher along the Y-direction than along the X-direction, as evidenced by the distance of heat transfer in both directions.

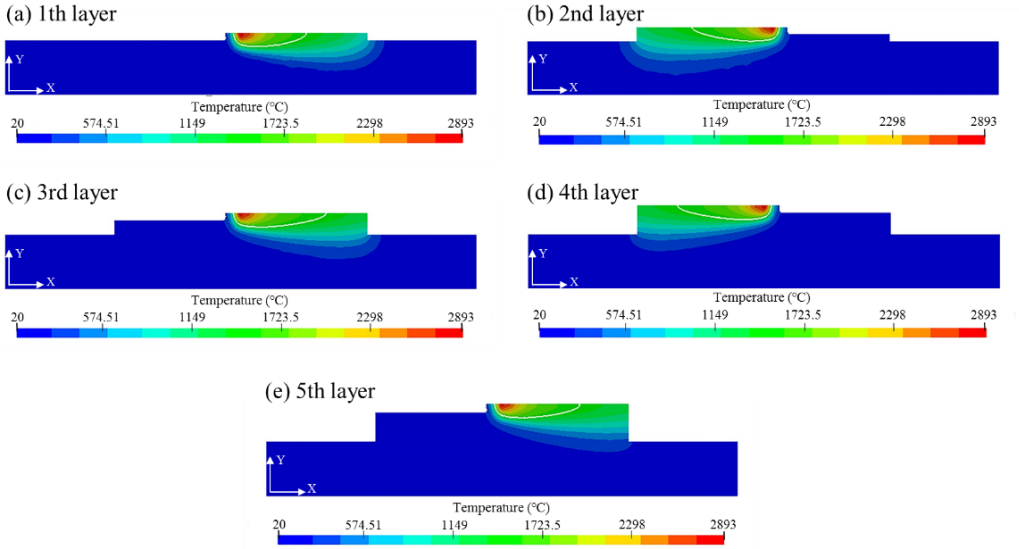


**Figure 3.** The temperature distribution: (a) 1th layer; (b) 2th layer; (c) 3th layer; (d) 4th layer; (e) 5th layer.

To systematically analyze the thermal history in the WAAM process, the thermal cycle of R1-R5 under different interlayer residence time is studied as shown in the figure 4, and the interlayer temperature of each layer is shown in the figure 5. In the thermal cycle curve of R1-R4, there are two temperature peaks higher than the melting temperature of 1450℃ at each position, indicating that remelting occurs and then solidification occurs again during the additive process. It is worth noting that the peak temperature in the R2 thermal cycle is as high as 2893℃ compared to the others. This is because there is heat accumulation in the additive process. As deposition proceeds, the previous layer of sediment is identified as the new substrate. Different interlayer residence time leads to different interlayer residence temperature, so the preheating temperature of the new substrate has been changing. The data for interlayer residence time and temperature are shown in figure 5. The shortest residence time between the second layer and the first layer is 70s, and the simulated interlayer temperature obtained is 164.339°C, resulting in relatively obvious heat accumulation in the deposition process of the second layer.

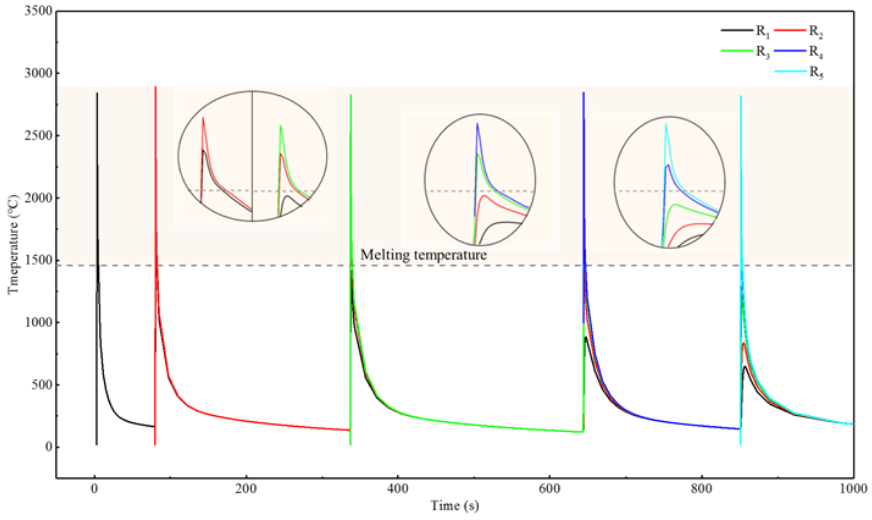


**Figure 4.** Temperature field and thermal cycle curve.

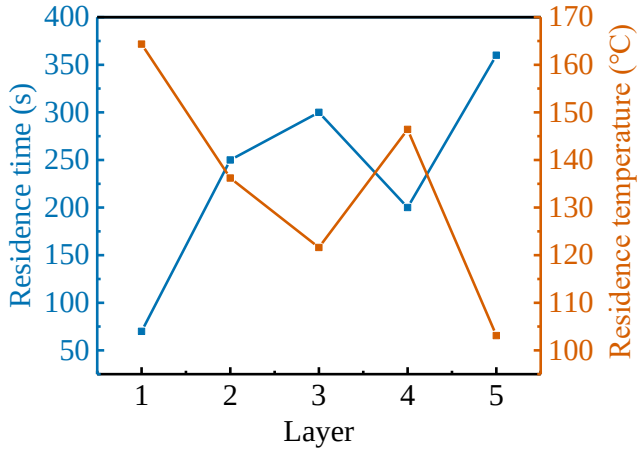


**Figure 5.** Interlayer residence time and temperature.

*4.3. Microstructure characteristic*

Figure 6 shows the microstructure of the stainless steel 316L straight wall. Figure 6(b)-figure 6(g) corresponds to the middle zone (zone A-zone E) of each layer and the top zone (zone F) of the fifth layer in figure 6(a), respectively. It can be clearly seen that the microstructure of the straight wall part is heterogeneous. A small number of cellular crystals appear in the lower part of the deposited layer (zone A), a small area at the top shows distinct equiaxed crystals and most of the area consists of columnar dendrites. It is well known that grain structure is closely related to the solidification parameters, which are mainly the temperature gradient (G) and solidification rate (R), calculated based on the equations (4)

and (5). The calculated results of the average temperature gradient and solidification rate for each region are shown in figure 7.Compared with the other five positions, the average temperature gradient in zone A of the first layer of straight-wall parts is higher, which is 651.595℃/mm, and the solidification rate is lower, which is 3.18377 mm/s. The reason is that the temperature of the initial substrate is lower than the temperature of the new substrate during the deposition process, resulting in a large temperature difference between the A zone near the substrate and the surrounding area during the deposition of the first layer. In addition, during the solidification process, the radiation and other heat dissipation conditions in the A zone, which is located near the bottom of the melt pool, are not as good as in the middle and top of the layers. In addition, during the solidification process, the heat dissipation conditions in the A area of the bottom of the straight wall part are not as good as in the middle and top of the straight wall part. The high temperature gradient and low solidification rate result in a relatively large G/R in zone A, which promotes the development of cellular crystals during solidification. In contrast, the grain structure at the top of the fifth layer (zone F) is equiaxed dendrites, which are formed under low G/R solidification conditions.

$$G = \|\nabla T\| = \left\| \frac{\partial T}{\partial x} i + \frac{\partial T}{\partial y} j + \frac{\partial T}{\partial z} k \right\| \tag{4}$$

$$R = v \cdot \vec{i} \cdot \vec{n} = v \cos\alpha \tag{5}$$

where, $\alpha$ is the angle between the arc deposition direction and the local solid-liquid front normal.

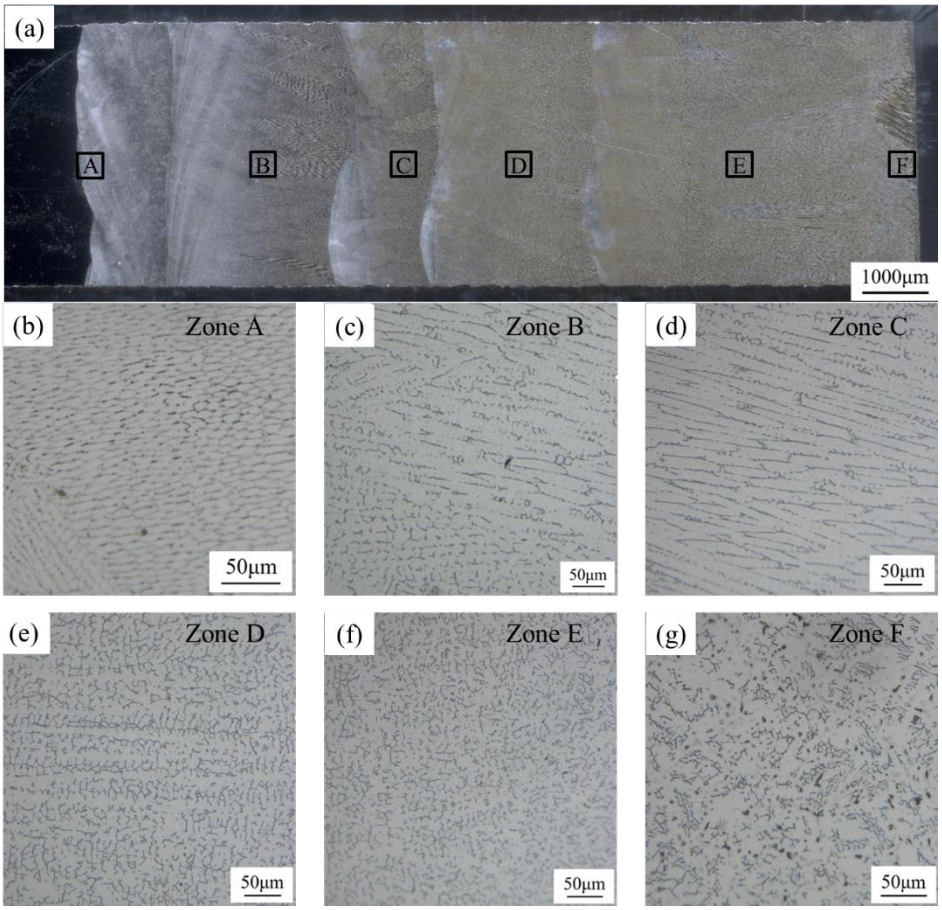


**Figure 6.** Optical micrographs of the microstructure of 316L: (a) the overall microstructure of the straight arm; (b) middle of 1st layer; (c) middle of 2nd layer; (d) middle of 3rd layer; (e) middle of 4th layer; (f) middle of 5th layer; (g) top of 5th layer.

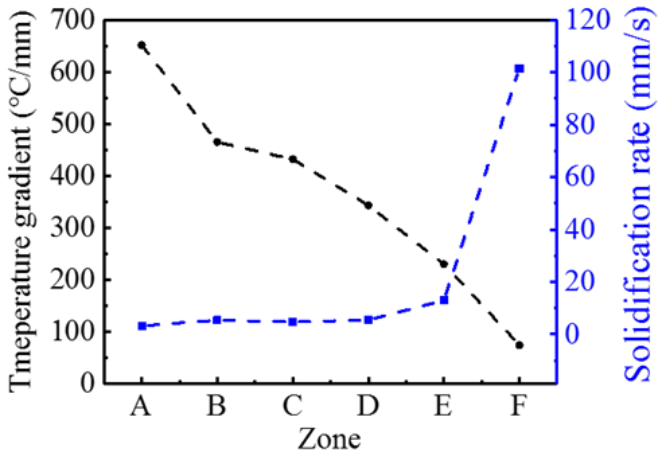


**Figure 7.** Temperature gradient and solidification rate in various zones.

## 5. Conclusions

In this study, the heat transfer behavior during the wire arc additive manufacturing of 316L stainless steel was investigated experimentally and by numerical calculations. The effect of interlayer residence time on the thermal cycle as well as the microstructure was analyzed. The main conclusions are as follows:

1. The finite element simulation results and thermocouple measurements match, verifying the accuracy of the model. In addition, the finite element model allows qualitative observation of the melting, solidification, reheating and remelting processes of the WAAM process.
2. The interlayer residence time influences the preheating temperature of the new substrate (interlayer residence temperature). With low interlayer residence time the preheating temperature of the new substrate leads to a more pronounced heat build-up.
3. In the solidification process of the wire arc additive manufacturing, the microstructure of the region with higher G/R is cellular crystals and columnar dendrites, and lower G/R tends to encourage the formation of equiaxed crystals.

## References

[1] Xiong Y B, Wen D X, Zheng Z Z and Li J J 2022 Effect of interlayer temperature on microstructure evolution and mechanical performance of wire arc additive manufactured 300M steel *Mater. Sci. Eng. A-Struct. Mater. Prop. Microstruct. Process*. **831** 13
[2] Lam T F, Xiong Y, Dharmawan A G, Foong S and Soh G S 2020 Adaptive process control implementation of wire arc additive manufacturing for thin-walled components with overhang features *Int. J. Adv. Manuf. Technol.* **108(4)** 1061-71
[3] Sachajdak A, Słoma J and Szczygieł I 2018 Thermal model of the gas metal arc welding hardfacing process *Applied Thermal Engineering* **141** 378-85
[4] Park J and Lee S H 2021 CMT-based wire arc additive manufacturing using 316L stainless steel (2): Solidification map of the multilayer deposit *Metals* **11**(11)
[5] Ge J G, Ma T J, Chen Y, Jin T N, Fu H G, Xiao R S, Lei Y P and Lin J 2019 Wire-arc additive manufacturing H13 part: 3D pore distribution, microstructural evolution, and mechanical performances *Journal of Alloys And Compounds* **783** 145-55
[6] Yin B, Ma H, Wang J, Fang K, Zhao H and Liu Y 2017 Effect of CaF 2 addition on macro/microstructures and mechanical properties of wire and arc additive manufactured Ti-6Al-4V components *Materials Letters* **190** 64-6
[7] Ding J, Colegrove P, Mehnen J, Ganguly S, Sequeira Almeida P M, Wang F and Williams S 2011 Thermo-mechanical analysis of wire and arc additive layer manufacturing process on large multi-layer parts *Computational Materials Science* **50** 3315-22
[8] Zhao H, Zhang G, Yin Z and Wu L 2011 A 3D dynamic analysis of thermal behavior during single-pass multi-layer weld-based rapid prototyping *Journal of Materials Processing Technology* **211**(3) 488-95

[9] Ogino Y, Asai S and Hirata Y 2018 Numerical simulation of WAAM process by a GMAW weld pool model *Welding in the World* **62**(2) 393-401
[10] Xiong J, Lei Y and Li R 2017 Finite element analysis and experimental validation of thermal behavior for thin-walled parts in GMAW-based additive manufacturing with various substrate preheating temperatures *Applied Thermal Engineering* **126** 43-52
[11] Lei Y, Xiong J and Li R 2018 Effect of inter layer idle time on thermal behavior for multi-layer single-pass thin-walled parts in GMAW-based additive manufacturing *The International Journal of Advanced Manufacturing Technology* **96** 1355-65
[12] Zhao Y, Jia Y, Chen S, Shi J and Li F 2020 Process planning strategy for wire-arc additive manufacturing: Thermal behavior considerations *Addit. Manuf.* **32** 100935
[13] Hejripour F, Binesh F, Hebel M and Aidun D K 2019 Thermal modeling and characterization of wire arc additive manufactured duplex stainless steel *Journal of Materials Processing Technology* **272** 58-71
[14] Ou W, Mukherjee T, Knapp G L, Wei Y and DebRoy T 2018 Fusion zone geometries, cooling rates and solidification parameters during wire arc additive manufacturing *International Journal of Heat and Mass Transfer* **127** 1084-94
[15] Huang J, Guan Z, Yu S, Yu X, Yuan W, Li N and Fan D A 2020 3D dynamic analysis of different depositing processes used in wire arc additive manufacturing *Materials Today Communications* **24** 101255
[16] Goldak J, Aditya C and Malcolm B 1984 A new finite element model for welding heat sources *Metallurgical transactions B* **15** 299-305

**Acknowledgments**
The authors gratefully thank the financial support by National Key R&D Program of China (No. 2018YFB1106501, 2018YFB1106505). The authors acknowledge the State Key Laboratory of Materials Processing and Die & Mould Technology of Huazhong University of Science and Technology.